Acta Crystallographica Section B
Structural Science
ISSN 0108-7681

Halogen···halogen interactions in pressure-frozen *ortho*- and *meta*-dichlorobenzene isomers

Maciej Bujak,[a] Kamil Dziubek[b] and Andrzej Katrusiak[b]*

[a]Institute of Chemistry, University of Opole, Oleska 48, 45-052 Opole, Poland, and [b]Faculty of Chemistry, Adam Mickiewicz University, Grunwaldzka 6, 60-780 Poznań, Poland

Correspondence e-mail: katran@amu.edu.pl

Received 29 September 2006
Accepted 6 November 2006

Isomers 1,2-dichlorobenzene (*o*-DCB) and 1,3-dichlorobenzene (*m*-DCB) were high-pressure frozen *in-situ* in a Merrill–Bassett diamond–anvil cell and their structures determined at room temperature and at 0.18 (5) GPa for *o*-DCB, and 0.17 (5) GPa for *m*-DCB by single-crystal X-ray diffraction. The patterns of halogen···halogen intermolecular interactions in these structures can be considered to be the main cohesive forces responsible for the molecular arrangements in these crystals. The molecular packing of dichlorobenzene isomers, including three polymorphs of 1,4-dichlorobenzene (*p*-DCB), have been compared and relations between their molecular symmetry, packing arrangements, intermolecular interactions and melting points discussed. The topology of the crystal packing in dichlorobenzene isomers results from the interplay of the molecular shape, steric hindrances and intermolecular interactions. The non-planar arrangement of the dichlorobenzene molecules in the crystal structures can be justified by the distributions of the electrostatic potential on molecular surfaces, which determines electrostatic intermolecular interactions.

1. Introduction

Dichlorobenzene isomers are convenient model compounds for studying the molecular packing, the role of weak intermolecular interactions and structure–property relations, such as the melting (freezing) temperature/pressure and compressibility of molecular crystals. Under ambient conditions only the D_{2h} symmetric 1,4-dichlorobenzene (*p*-DCB) is solid (melting point 325.8 K), whereas the C_{2v} symmetric 1,2-dichlorobenzene (*o*-DCB) and 1,3-dichlorobenzene (*m*-DCB) isomers are liquids freezing at 256.4 and 248.3 K, respectively. The boiling points of all dichlorobenzenes are very similar, with a difference of only *ca* 7 K between the highest boiling temperature (of *o*-DCB) from the lowest one (of *m*-DCB; Lide, 1994). It is a common feature that boiling points of isomers exhibit much smaller differences which usually are not correlated to the melting points.

Several rules relating the molecular structure and the melting point of substances for molecular crystals with van der Waals interactions and without strong specific cohesion forces have been formulated. The trends of the melting point of substances rising in homologous series with molecular weight (Austin, 1930), and for the increasingly symmetrical and more compact molecules were already observed (Holler, 1947; Brown & Brown, 2000) and partly explained. Among isomeric organic substances, the higher melting point of the more symmetrical isomer was attributed to the thermodynamic relation

$$T_m = \Delta H_m/\Delta S_m,$$

where the higher enthalpy of melting, ΔH_m, the lower entropy of melting, ΔS_m, or a combination of these two factors are associated with the higher molecular symmetry. Boese *et al.* (2001) determined the low-temperature crystal structures of *o*-DCB and *m*-DCB and computed the packing energies for all dichlorobenzene isomers. They concluded that the melting points correlate with the energies of crystal packing, which in turn depend on the molecular shape and symmetry. The recent study on the analysis of the molecular van der Waals symmetry afforded a theoretical interpretation of the observed $T_{meta} < T_{ortho} < T_{para}$ melting-point sequence in disubstituted benzenes (Slovokhotov *et al.*, 2004).

While the crystal structures of *o*-DCB and *m*-DCB remained unknown until 2001, the structures of all α, β and γ phases of *p*-DCB have been widely studied since 1952 (Croatto *et al.*, 1952; Frasson *et al.*, 1959; Housty & Clastre, 1957; Wheeler & Colson, 1975, 1976; Estop *et al.*, 1997; Ibberson & Wilson, 2002). At ambient pressure and at *ca* 328 K, *p*-DCB crystallizes in the high-temperature triclinic β phase (space group $P\bar{1}$, $Z = 1$). At *ca* 304 K it transforms to the room-temperature monoclinic α phase ($P2_1/a$, $Z = 2$). Below *ca* 273 K, *p*-DCB crystallizes in the low-temperature monoclinic γ phase ($P2_1/c$, $Z = 2$). An orthorhombic δ phase of *p*-DCB was also reported by Sankaran *et al.* (1986), however, Ibberson & Wilson (2002) did not find any experimental evidence of its existence. One year later, an orthorhombic structure in the space group *Abma* corresponding to the δ phase, was postulated theoretically for *p*-DCB under a pressure of 0.3 GPa and at 295 K (Thiéry & Rérat, 2003).

Wheeler & Colson (1976) examined Cl···Cl distances shorter than 3.9 Å in the structures of *p*-DCB polymorphs α, β (both supercooled) and γ determined at 100 K and ambient pressure. They found three Cl···Cl contacts in the β phase, and four and five contacts in forms α and γ, respectively. The same sequence (β, α and γ) of the packing energy (thermodynamic stability) of these three phases was discussed. It should be emphasized that a very short and almost linear C—Cl···Cl—C contact of 3.38 Å was found only in the structure of the β phase. The authors, on the basis of the calculated isotropic Buckingham atom–atom potentials, found that this contact should be associated with repulsive interactions. On the other hand, the anisotropic atom–atom potential model reproduces well even such short distances (Day & Price, 2003). Moreover, in crystalline chlorine at ambient pressure the shortest intermolecular Cl···Cl distance, depending on temperature, ranges from 3.26 (22 K) to 3.33 Å (160 K; Stevens, 1979; Powell *et al.*, 1984).

Recently we investigated the high-pressure crystal structures and transformations of two chloro derivatives of ethane: 1,2-dichloroethane (Bujak *et al.*, 2004) and 1,1,2,2-tetrachloroethane (Bujak & Katrusiak, 2004). Each of these compounds forms two crystal phases, α and β, with the ethylene moieties ordered and disordered. It was observed that the transitions between these phases considerably modify the geometry of the Cl···Cl contacts in their structures. Thus, it appeared that the internal conformational disorder competes with the specific intermolecular Cl···Cl interactions. On the other hand, it can be argued that the densely packed molecules interact with their outermost atoms and these interactions change when the molecules and structures transform. From this point of view, the Cl···Cl contacts can be regarded as a natural consequence of the atomic location in molecules, and are not caused by significant differences between the energies of the Cl···Cl and other van der Waals interactions (*e.g.* Grineva & Zorkii, 1998, 2001).

The present investigation of *ortho*- and *meta*-dichlorobenzenes continues our study of the pressure-freezing and structure–property relations of halogenated molecular crystals. The role of halogen···halogen contacts for the crystal cohesive forces, their influence on the crystal and molecular structure and on the melting (freezing) temperature/pressure, as well as the comparison of the low-temperature and high-pressure crystal structures are the main purposes of this report.

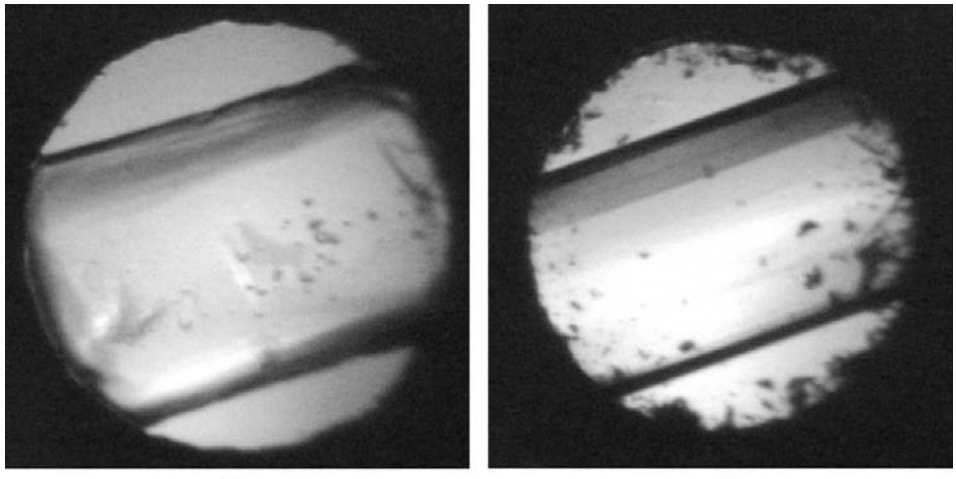

(*a*) (*b*)

Figure 1
Single crystals, in the form of a prism, in the high-pressure diamond–anvil cell at 295 K (*a*) and 0.18 GPa for *o*-DCB, and (*b*) 0.17 GPa for *m*-DCB.

2. Experimental

Commercially available 1,2-dichlorobenzene, *o*-DCB (POCh, Poland) and 1,3-dichlorobenzene, *m*-DCB (BDH Laboratory Chemicals Division, England), were used without further purification. The single crystals of these compounds were crystallized *in situ* in a Merrill–Bassett diamond–anvil cell, DAC (Merrill & Bassett, 1974). A description of the pres-

Table 1
Crystal data and details of the structure refinement for *o*-DCB and *m*-DCB.

	o-DCB	*m*-DCB
Crystal data		
Pressure (GPa)	0.18 (5)	0.17 (5)
Temperature (K)	295 (2)	295 (2)
Chemical formula	$C_6H_4Cl_2$	$C_6H_4Cl_2$
M_r	146.99	146.99
Cell setting, space group	Monoclinic, $P2_1/n$	Monoclinic, $P2_1/c$
a, b, c (Å)	3.9274 (4)	3.9163 (6)
	10.5678 (10)	12.532 (5)
	15.199 (9)	25.849 (5)
β (°)	96.70 (2)	93.098 (14)
V (Å^3)	626.5 (4)	1266.8 (6)
Z	4	8
D_x (Mg m^{-3})	1.558	1.541
Radiation type (Å)	0.71073	0.71073
μ (mm^{-1})	0.91	0.90
Crystal form, color	Prism, colorless	Prism, colorless
Crystal size (mm)	0.44 × 0.44 × 0.12	0.40 × 0.40 × 0.12
Data collection		
Diffractometer	Kuma KM4-CCD κ geometry	Kuma KM4-CCD κ geometry
Data collection method	φ and ω scans	φ and ω scans
Absorption correction	Analytical	Analytical
T_{min}	0.43	0.40
T_{max}	0.79	0.82
No. of measured, independent and observed reflections	3835, 431, 133	4205, 800, 627
Criterion for observed reflections	$I > 2\sigma(I)$	$I > 2\sigma(I)$
R_{int}	0.069	0.091
θ_{max} (°)	24.96	24.98
Refinement		
Refinement on	F^2	F^2
$R[F^2> 2\sigma(F^2)]$, $wR(F^2)$, S	0.031, 0.037, 0.63	0.109, 0.129, 1.47
No. of reflections	431	800
No. of parameters	73	146
H-atom treatment	Constrained refinement	Constrained refinement
Weighting scheme	$w = 1/[\sigma^2(F_o^2) + (0.0138P)^2]$, where $P = (F_o^2 + 2F_c^2)/3$	$w = 1/[\sigma^2(F_o^2) + (0.0230P)^2 + 1.956P]$, where $P = (F_o^2 + 2F_c^2)/3$
$(\Delta/\sigma)_{max}$	< 0.0001	< 0.0001
$\Delta\rho_{max}$, $\Delta\rho_{min}$ (e Å^{-3})	0.206, −0.217	0.176, −0.186
Extinction method	None	*SHELXL*
Extinction coefficient	–	0.018 (2)

Computer programs used: *CrysAlisCCD*, *CrysAlisRED* (Oxford Diffraction, 2004), *REDSHABS* (Katrusiak, 2003), *SHELXS*97, *SHELXL*97 (Sheldrick, 1997), *SHELXTL* (Sheldrick, 1990).

sure-freezing method was reported earlier (*e.g.* Fourme, 1968; Vos *et al.*, 1993; Bujak *et al.*, 2004). The diameter of the diamond culets was 0.8 mm. The gasket was made of 0.2 mm thick Inconel foil with a spark-eroded 0.5 mm hole (Katrusiak, 1999). *o*-DCB froze at *ca* 0.18 (5) GPa, whereas *m*-DCB froze at the slightly lower pressure of *ca* 0.17 (5) GPa. Both for *o*-DCB and *m*-DCB, the pressure-frozen polycrystalline sample was heated using a hot-air gun until all crystallites melted except one. This crystal seed was allowed to grow, giving the single crystal for both *o*-DCB and *m*-DCB in a similar form, that of a prism (Fig. 1). The pressure in a DAC was determined from the shift of the R_1 fluorescence line of a small ruby chip (Piermarini *et al.*, 1975), using a BETSA PRL spectrometer, with the accuracy of *ca* 0.05 GPa.

The single crystals of *o*-DCB and *m*-DCB were centred on a diffractometer (graphite-monochromated Mo *Ka* radiation) by the gasket-shadowing method (Budzianowski & Katrusiak, 2004). Intensity data were collected with $\Delta\omega = 1.0°$ scan mode, and exposure times of 30 s for *o*-DCB and 40 s for *m*-DCB. The data were corrected for Lorentz–polarization effects and for the absorption of the X-rays by the DAC, shadowing the crystal by the gasket edges and absorption of the sample (Katrusiak, 2003, 2004). The transmission of the DAC varied between 0.63 and 0.90 for *o*-DCB and 0.62 and 0.93 for *m*-DCB, and of the crystal itself varied between 0.88 and 0.90 for *o*-DCB and 0.88 and 0.90 for *m*-DCB. Both structures were solved by direct methods. The Cl and C atoms were refined with anisotropic displacement parameters. The H atoms were located from molecular geometry (a C—H distance of 0.93 Å was applied). The U_{iso} parameters of the H atoms were assumed to be 1.2 times larger than the U_{eq} parameters of their carriers. The *CrysAlisCCD* and *CrysAlisRED* programs (Oxford Diffraction, 2004) were used for the data collection, unit-cell refinement and initial data reduction processes. The unit-cell setting and space group $P2_1/n$ of *o*-DCB were chosen in accordance with the previous determination of the isostructural low-temperature phase of this compound (Boese *et al.*, 2001). The solution and refinement of the structures were carried out with the *SHELX*97 program (Sheldrick, 1997). The structural drawings were prepared using the *XP* program (Sheldrick, 1990). The crystallographic data have been listed in Table 1.[1] The shadowing of the sample by the gasket was from 0.77 to 0.98 for *o*-DCB and from 0.73 to 0.98 for *m*-DCB.

Geometry optimization and the subsequent calculations of the electrostatic potentials mapped onto the molecular surfaces of dichlorobenzene isomers were run on a PC using the *GAUSSIAN*03 program package (Frisch *et al.*, 2003). The DFT calculations were performed at the B3LYP/6-311++g(d,p) level of theory. The molecular surfaces were defined following Bader *et al.* (1987) as 0.001 a.u. electron-density envelopes.

[1] Supplementary data for this paper are available from the IUCr electronic archives (Reference: SO5006). Services for accessing these data are described at the back of the journal.

Table 2
Selected molecular dimensions (Å, °) and Cl···Cl contacts (Å) for the structure of *o*-DCB at 295 K and 0.18 GPa, and *m*-DCB at 295 K and 0.17 GPa.

The two symmetry-independent molecules in the *m*-DCB crystal have been denoted with letters (*a*) and (*b*).

o-DCB		*m*-DCB (*a*)		*m*-DCB (*b*)	
C1—Cl1	1.71 (2)	C1—Cl1	1.739 (17)	C7—Cl3	1.761 (13)
C1—C2	1.376 (18)	C1—C2	1.380 (13)	C7—C8	1.383 (11)
C1—C6	1.342 (10)	C1—C6	1.373 (13)	C7—C12	1.357 (15)
C2—Cl2	1.704 (9)	C3—Cl2	1.719 (12)	C9—Cl4	1.741 (11)
C2—C3	1.403 (19)	C2—C3	1.362 (15)	C8—C9	1.384 (13)
C3—C4	1.391 (11)	C3—C4	1.368 (12)	C9—C10	1.372 (15)
C4—C5	1.359 (16)	C4—C5	1.382 (13)	C10—C11	1.369 (11)
C5—C6	1.379 (17)	C5—C6	1.360 (16)	C11—C12	1.383 (13)
C1—C2—Cl2	124.7 (13)	C2—C3—Cl2	119.2 (9)	C8—C9—Cl4	116.8 (11)
C1—C2—C3	116.8 (11)	C1—C2—C3	120.1 (12)	C7—C8—C9	114.8 (12)
C1—C6—C5	118.2 (14)	C1—C6—C5	117.5 (13)	C7—C12—C11	119.0 (12)
C2—C1—Cl1	117.3 (9)	C2—C1—Cl1	119.5 (10)	C8—C7—Cl3	116.8 (11)
C3—C2—Cl2	118.4 (9)	C4—C3—Cl2	120.6 (11)	C10—C9—Cl4	119.4 (9)
C4—C3—C2	120.6 (14)	C4—C3—C2	120.1 (11)	C10—C9—C8	123.8 (12)
C4—C5—C6	121.8 (9)	C4—C5—C6	122.7 (13)	C10—C11—C12	120.2 (14)
C5—C4—C3	118.8 (14)	C5—C4—C3	118.6 (14)	C11—C10—C9	118.5 (12)
C6—C1—Cl1	118.9 (14)	C6—C1—Cl1	119.4 (10)	C12—C7—Cl3	119.5 (9)
C6—C1—C2	123.7 (17)	C6—C1—C2	121.1 (15)	C12—C7—C8	123.7 (12)
Cl1···Cl2	3.134 (7)	Cl2···Cl3^{iii}	3.669 (6)	Cl3···Cl2^{iv}	3.669 (6)
Cl1···Cl2^{i}	3.573 (4)			Cl4···Cl4^{v}	3.434 (5)
Cl2···Cl1^{ii}	3.573 (4)				

Symmetry codes: (i) $-\frac{1}{2}+x, -\frac{1}{2}+y, \frac{3}{2}-z$; (ii) $-\frac{1}{2}+x, \frac{1}{2}+y, \frac{3}{2}-z$; (iii) $-1+x, -1+y, z$; (iv) $1+x, 1+y, z$; (v) $1-x, 2-y, -z$.

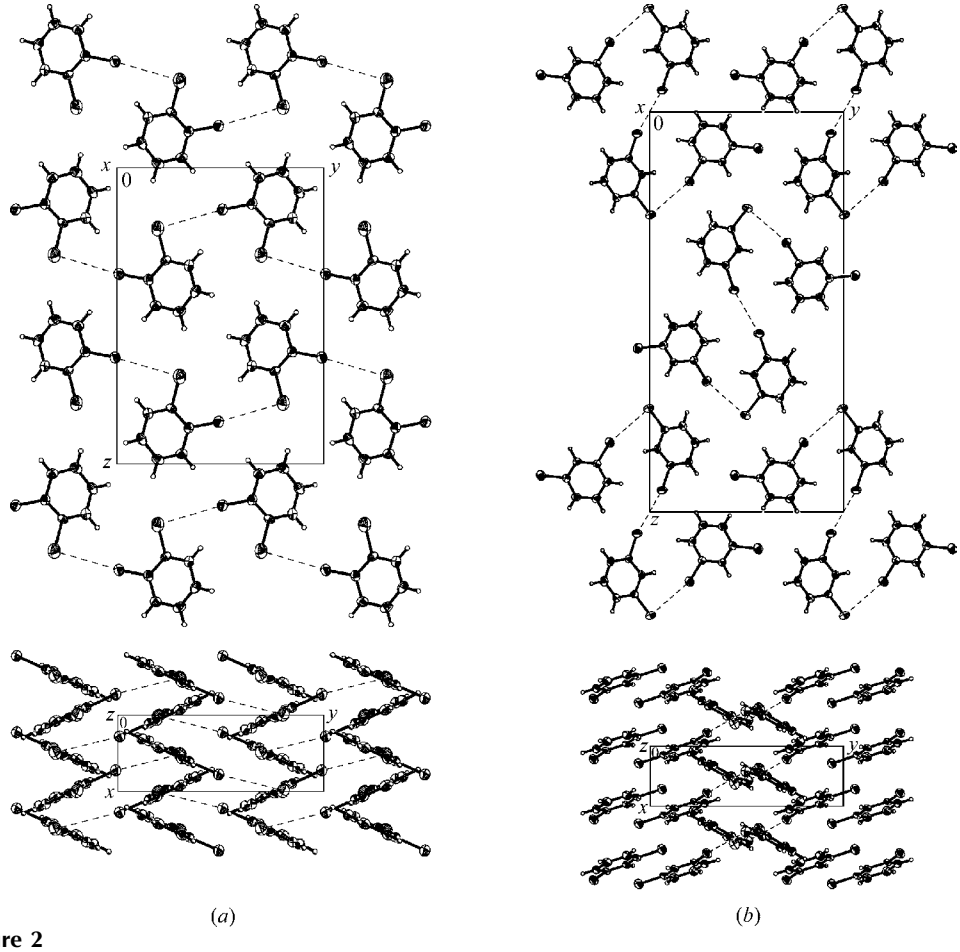

Figure 2
Crystal structures of (*a*) *o*-DCB at 295 K and 0.18 GPa, and (*b*) *m*-DCB at 295 K and 0.17 GPa. Displacement ellipsoids are plotted at the 25% probability level. The broken lines denote Cl···Cl intermolecular contacts.

3. Results

3.1. X-ray structures

The pressure-frozen *o*-DCB and *m*-DCB crystals obtained in this study are isostructural with those temperature-frozen at ambient pressure (Boese *et al.*, 2001). The crystals of both dichlorobenzene isomers are monoclinic and centrosymmetric. The space group of *o*-DCB is $P2_1/n$, $Z = 4$ and there is one symmetry-independent molecule in the unit cell. The space group of *m*-DCB is $P2_1/c$, $Z = 8$ and there are two symmetry-independent molecules (Table 1). Both these structures can be considered as built of corrugated layers of dichlorobenzene molecules forming Cl···Cl dihalogen contacts (Fig. 2). In the *o*-DCB structure at 0.18 GPa the Cl1 and Cl2 atoms are each involved in one intermolecular contact of 3.573 (4) Å (Fig. 3*a*, Table 2). Thus, each molecule forms two Cl···Cl contacts arranging the molecules into a one-dimensional zigzag-like chain along [010]. In the *m*-DCB structure four molecules interacting by relatively short Cl···Cl contacts of 3.669 (6) and 3.434 (5) Å between Cl2^{iii} and Cl3^{v} (Cl3 and Cl2^{iv}), and Cl4 and Cl4^{v} atoms, respectively (Fig. 3*b*, Table 2), form a group with no other short Cl···Cl contacts to their neighbors. The Cl1 atom, in the structure of *m*-DCB, is not engaged in any Cl···Cl interactions and its shortest intermolecular distance of this type is 3.92 Å.

The separation between centroids of the aromatic rings is very similar in both structures, of 3.927 and 3.916 Å for *o*-DCB and *m*-DCB, respectively. These distances (equal to the lengths of the unit-cell parameters *a*) are similar to those found at 100 K and ambient pressure in

the structures of *p*-DCB polymorphs α and β: 3.925 and 3.882 Å, respectively (in *p*-DCB α and β are equal to the unit-cell parameters *c*). In the γ phase of *p*-DCB, at 100 K and ambient pressure the shortest distance between the ring centroids (4.775 Å) is considerably longer. The angles between molecular planes of neighboring molecules in the *o*-DCB and *m*-DCB structures, of 51.58 (6) and 49.51 (15)°, are almost identical to those (51.36 and 49.42°, respectively) in the low-temperature structures of these isomers (Boese *et al.*, 2001). The values are also within the range between 57.6 and 48.4° found at 100 K and ambient pressure for the α and γ phases of *p*-DCB (Wheeler & Colson, 1976). There are no significant distortions from planarity of the *o*-DCB and *m*-DCB molecules. The average C—C bond distances are all equal within experimental error. The average bond length of 1.375 Å for *o*-DCB, and 1.371 and 1.375 Å for the two symmetry-independent molecules in *m*-DCB, are not significantly different from the average bond length found in the high-pressure structure of benzene determined at room temperature and 0.30 GPa (1.39 Å; Budzianowski & Katrusiak, 2006) and in all three ambient-pressure phases of *p*-DCB (Wheeler & Colson, 1976). The C—Cl bond lengths (mean 1.707 Å for *o*-DCB, and 1.729 and 1.751 Å for *m*-DCB) are also similar to those found in their low-temperature structures (Boese *et al.*, 2001) and in *p*-DCB.

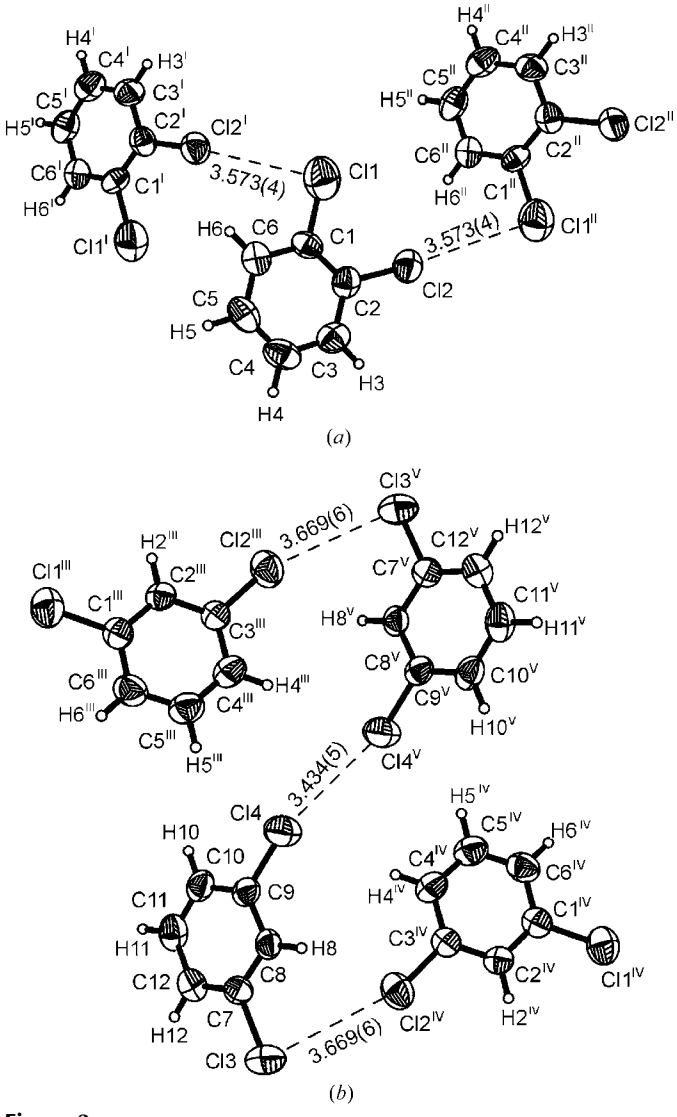

Figure 3
Intermolecular Cl···Cl interactions in the structure of (*a*) *o*-DCB at 295 K and 0.18 GPa, and (*b*) *m*-DCB at 295 K and 0.17 GPa, denoted by broken lines. Displacement ellipsoids are plotted at the 50% probability level. Symmetry codes: (i) $-\frac{1}{2}+x, -\frac{1}{2}+y, \frac{3}{2}-z$; (ii) $-\frac{1}{2}+x, \frac{1}{2}+y, \frac{3}{2}-z$; (iii) $-x, 1-y, -z$; (iv) $1+x, 1+y, z$; (v) $1-x, 2-y, -z$.

3.2. Computational analysis

The concept of anisotropic intermolecular Cl···Cl contacts has been applied for analysing the molecular packing of dichlorobenzene isomers. Nyburg & Faerman (1985) postulated an elliptic effective van der Waals radius of chlorine (1.58 Å for head-on *versus* 1.78 Å for side-on contacts), whereas Price *et al.* (1994) attributed this anisotropy to the non-spherical atomic charge distribution. By using this approach Day & Price (2003) applied an anisotropic atom–atom energy-potential model and successfully reproduced the crystal structures of various chlorobenzenes (from one to six Cl atoms per molecule), including all the known phases of dichlorobenzene isomers. The short intermolecular Cl···Cl distances in their predicted structures are consistent with those crystal structures determined by X-rays. While in the structure of *o*-DCB the Cl···Cl contacts are of the type II (one C—Cl···Cl angle is *ca* 90° and the other *ca* 180°), in the structure of *m*-DCB the longer contact of 3.669 (6) Å is of type II, and the shorter one, 3.434 (5) Å, is of the type I characterized by an almost linear arrangement of atoms C—Cl···Cl—C (Desiraju & Parthasarathy, 1989). The difference between these Cl···Cl distances in *m*-DCB of 0.235 Å is only slightly larger than the span between the minor and major Cl radii (Nyburg & Faerman, 1985). The non-covalent interactions can also be related to the electrostatic potential on the molecular surface. It appears that in both aromatic and aliphatic systems, the distribution of the molecular electrostatic potential is similar: it is negative around the C—Cl bond with a small positive cap at the extension of the C—Cl bond (Murray *et al.*, 1994; Brammer *et al.*, 2001; Politzer *et al.*, 2002). Murray *et al.* (1994) calculated the electrostatic potential and also plotted it on the molecular surface for the mono-

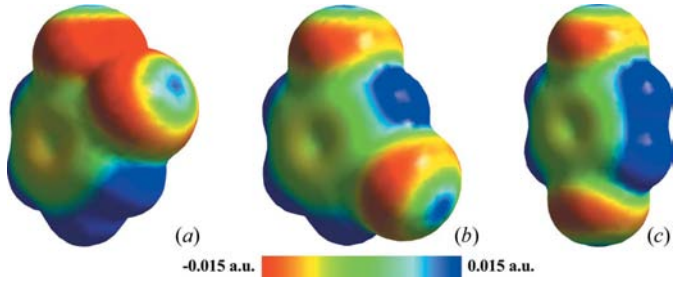

Figure 4
Molecular isodensity surfaces for (*a*) *o*-, (*b*) *m*- and (*c*) *p*-DCB isomers mapped with their electrostatic potential. The potential ranges from −0.015 a.u. (red) to 0.015 a.u. (blue).

substituted benzene derivatives. Apart from distinguishing between the benzene derivatives with electron-donating and electron-withdrawing substituents, they concluded that monohalogenated benzenes form a third distinct group. Its peculiarity, which also manifests itself in the anomalous reactivity in an electrophilic substitution reaction, could be attributed to the fact that the halogens are both electronegative and have electron lone pairs, so the net result is the combination of inductive and resonance contributions. According to the alternative theory, this behavior may arise from the unique energy level of the halogen lone-pair orbital, which is higher than the adjacent π-molecular orbital of benzene (Tomoda *et al.*, 1998). Apart from the unusual potential anisotropy about the Cl atom, in the halogenated benzenes a small negative potential is located on both sides of the aromatic ring plane, which facilitates weak electrophilic interactions, *e.g.* with H atoms. Similar electrostatic potential distributions have been found by our *ab initio* calculations for the dichlorobenzene molecules (Fig. 4). Besides, the potential on the molecular surface around the C—Cl bond is apparently more negative in the regions perpendicular to the aromatic ring plane. This feature, common for all dichlorobenzene isomers, is a likely reason for the non-planarity of the molecular aggregates (chains in *o*-DCB and tetramers in *m*-DCB) formed by the Cl···Cl association. It is remarkable that this differentiation of electrostatic potential increases from *o*-DCB to *p*-DCB. The distribution of negative potential perpendicular to the C—Cl bond and to the molecular plane is also similar in the monochlorobenzene molecule.

3.3. Structure – melting-point relation

It has been shown that the differences between the thermodynamic stabilities and melting (freezing) points of the *o*-DCB, *m*-DCB and *p*-DCB polymorphs can be rationalized, on a molecular level, by the molecular symmetry and by the number and character of intermolecular interactions in their crystal structures.

The intermolecular interactions in the structures of *o*-DCB and *m*-DCB, visualized on the Hirshfeld surfaces (Wolff *et al.*, 2005; McKinnon *et al.*, 2004), are almost identical for the low-temperature (Boese *et al.*, 2001) and high-pressure structures reported in this work. Therefore, only the intermolecular contacts in the high-pressure structures of *o*-DCB and *m*-DCB and, for comparison, the three low-temperature structures of all the polymorphs of *p*-DCB have been discussed (Figs. 5 and 6).

The *p*-DCB is more tightly packed than the other isomers and it shows a lower lattice energy for the calculated structures in all the space groups considered (Boese *et al.*, 2001). The tight packing of *p*-DCB may result from a molecular geometry factor. In the *para* isomer the Cl atoms are least hindered and most accessible for Cl···Cl interactions (Wheeler & Colson, 1976). The steric hindrances in *o*-DCB and *m*-DCB are likely to be responsible for the DCB molecules being engaged in at most two Cl···Cl

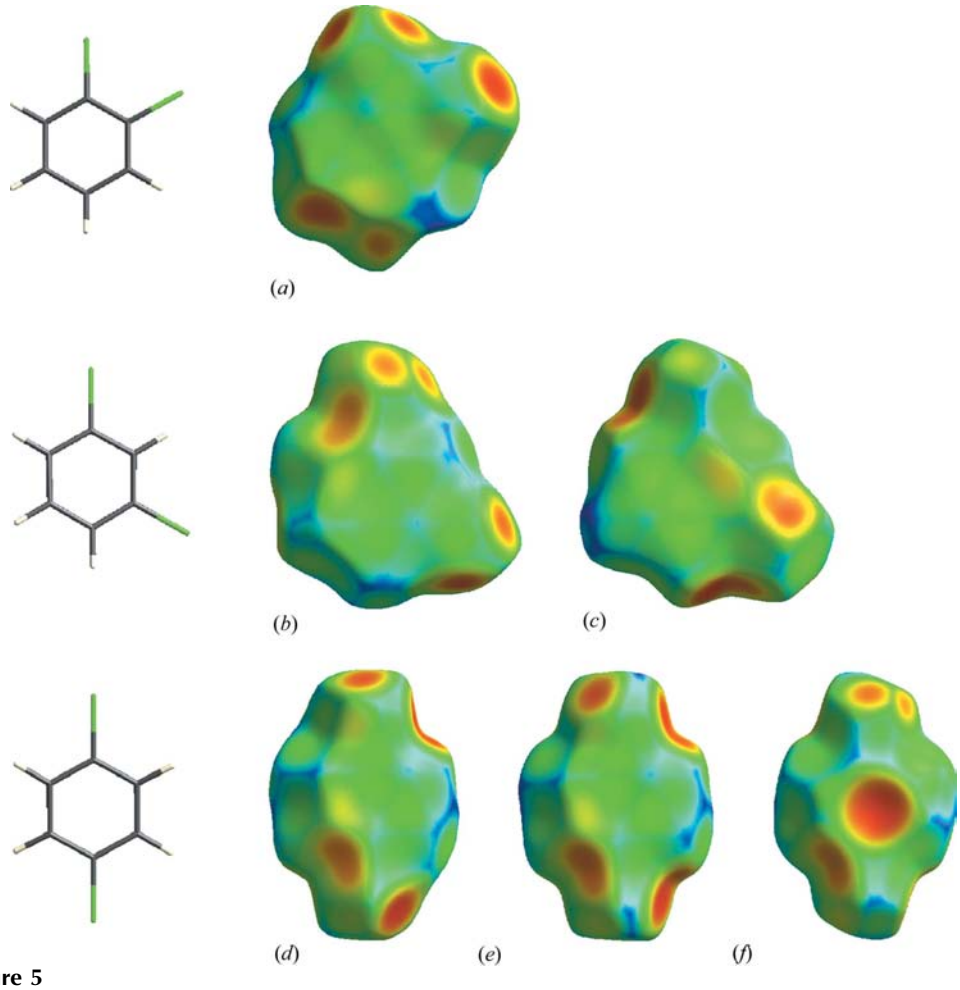

Figure 5
Hirshfeld surfaces for the room-temperature high-pressure structures of (*a*) *o*-DCB, (*b*)–(*c*) *m*-DCB, as well as the low-temperature ambient-pressure structures of (*d*)–(*f*) α, β and γ polymorphs of *p*-DCB (Wheeler & Colson, 1976). The red color represents the closest and blue the most distant contacts from the surface to the nearest atom external to the surface. Pictures (*b*) and (*c*) represent two symmetry-independent molecules in the structure of *m*-DCB.

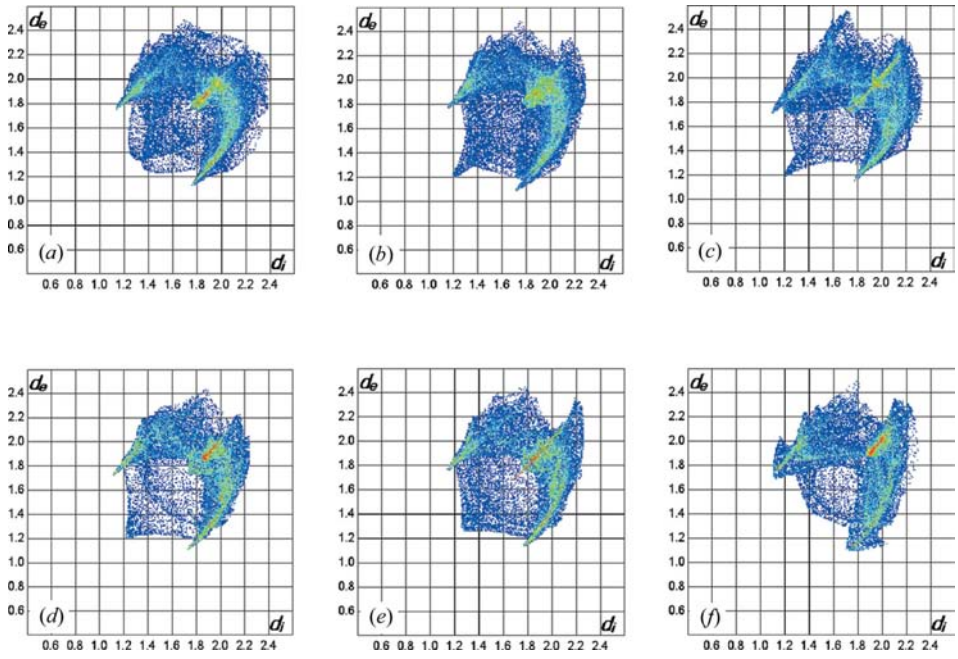

Figure 6
Two-dimensional fingerprint plots for the room-temperature high-pressure structures of (*a*) *o*-DCB, (*b*)–(*c*) *m*-DCB as well as the low-temperature ambient-pressure structures of (*d*)–(*f*) α, β and γ polymorphs of *p*-DCB (Wheeler & Colson, 1976). Two separate plots (*b* and *c*) for two symmetry-independent molecules in the structure of *m*-DCB are presented.

interactions (Boese *et al.*, 2001), as can be seen in Figs. 2 and 3. The difference in packing is manifested by the number of red points in the two-dimensional fingerprint plots for *o*-DCB and *m*-DCB (Figs. 5*a*–*c*) compared with the plots for all the *p*-DCB phases (Figs. 6*d*–*f*).

When exploring the packing modes and intermolecular contacts in the structures of the α, β and γ polymorphs of *p*-DCB, the similarities of their character for the α and β forms, and the distinctly different packing in the γ polymorph should be emphasized. Apart from the Cl$\cdots$Cl interactions, discussed by Boese *et al.* (2001), all three polymorphs display relatively long C—H$\cdots$Cl contacts (the closest of *ca* 2.8 Å). Additional short contacts of the C—H$\cdots\pi$ type are only formed in the most stable γ polymorph. At the same time, the H$\cdots$H contacts are significantly shorter in the α form than in forms β and γ, as can be observed from the scale of distances on the Hirshfeld surfaces (Spackman & McKinnon, 2002; Figs. 5 and 6*d*–*f*). This analysis of intermolecular interactions is consistent with the sequence of thermodynamic stability of the *p*-DCB polymorphs at 100 K (Wheeler & Colson, 1976).

The molecular packing patterns and intermolecular interactions (illustrated on the Hirshfeld surfaces and their two-dimensional fingerprint plots in Figs. 5 and 6*a*–*c*) can be correlated with the thermodynamic stability and melting points of *o*-DCB and *m*-DCB. The higher melting point of the isomer *o*-DCB corresponds to its Cl$\cdots$Cl interactions being more pronounced than in *m*-DCB. In the *m*-DCB structure one Cl atom is not involved in any Cl$\cdots$Cl interactions and the molecules form isolated tetramers, in contrast to the more energetically favorable (*i.e.* satisfying more Cl$\cdots$Cl contacts) zigzag chains in the structure of *o*-DCB. The shortest Cl4$\cdots$Cl4^{V} I-type contact (Fig. 3*b*, Table 2) in the structure of *m*-DCB of 3.434 (5) Å is clearly visible in Fig. 5(*c*). Expanding the investigation carried by Wheeler & Colson (1976), the number and uniform distribution of contacts (*i.e.* similar Cl$\cdots$Cl length, as opposed to uneven distances – short and long ones) is consistent with the crystal stability. Moreover, in the *o*-DCB and *m*-DCB isomers there are no C—H$\cdots\pi$ contacts similar to those in the γ phase of *p*-DCB. The area coverage and the density of points on the fingerprint plots (Fig. 6*a*–*c*) facilitate the analyses of specific types of interactions, however, their relation to the stability of crystal structures is not straightforward.

4. Conclusions

The low-temperature and high-pressure freezing processes of *ortho*- and *meta*-dichlorobenzene isomers led to the same phases of these compounds. On the molecular level, the differences in freezing pressures and freezing (melting) temperatures of the dichlorobenzene isomers can be attributed to the locations of their substituents and their role in the formation of intermolecular interactions. Apart from the Cl$\cdots$Cl contacts, other interactions also contribute to the stability of the crystal structures. It appears that on the structural level the freezing (melting) temperature and pressure depend mainly on the packing efficiency of the isomers. The entropy of melting is reduced by high molecular symmetry because it is likely to allow more tight packing in the crystalline state. From the point of view of the role of molecular symmetry for the freedom gained upon melting, the symmetrical molecules have fewer (but more degenerate) orientational states compared with the molecules of a lower symmetry. It has been shown that the crystal packing of DCB isomers is partly governed by electrostatic interactions, favoring staggered (as opposed to coplanar) arrangements of molecules forming short Cl$\cdots$Cl contacts.

References

Austin, J. B. (1930). *J. Am. Chem. Soc.* **52**, 1049–1053.
Bader, R. F. W., Carroll, M. T., Cheeseman, J. R. & Chang, C. (1987). *J. Am. Chem. Soc.* **109**, 7968–7979.
Boese, R., Kirchner, M. T., Dunitz, J. D., Filippini, G. & Gavezzotti, A. (2001). *Helv. Chim. Acta*, **84**, 1561–1577.
Brammer, L., Bruton, E. A. & Sherwood, P. (2001). *Cryst. Growth Des.* **1**, 277–290.
Brown, R. J. C. & Brown, R. F. C. (2000). *J. Chem. Educ.* **77**, 724–731.
Budzianowski, A. & Katrusiak, A. (2004). *High-Pressure Crystallography*, edited by A. Katrusiak & P. F. McMillan, pp. 101–112. Dordrecht: Kluwer Academic Publishers.
Budzianowski, A. & Katrusiak, A. (2006). *Acta Cryst.* B**62**, 94–101.
Bujak, M., Budzianowski, A. & Katrusiak A. (2004). *Z. Kristallogr.* **219**, 573–579.
Bujak, M. & Katrusiak, A. (2004). *Z. Kristallogr.* **219**, 669–674.
Croatto, U., Bezzi, S. & Bua, E. (1952). *Acta Cryst.* **5**, 825–829.
Day, G. M. & Price, S. L. (2003). *J. Am. Chem. Soc.* **125**, 16434–16443.
Desiraju, G. R. & Parthasarathy, R. (1989). *J. Am. Chem. Soc.* **111**, 8725–8726.
Estop, E., Alvarez-Larena, A., Belaaraj, A., Solans, X. & Labrador, M. (1997). *Acta Cryst.* C**53**, 1932–1935.
Fourme, R. (1968). *J. Appl. Cryst.* **1**, 23–30.
Frasson, E., Garbuolio, C. & Bezzi, S. (1959). *Acta Cryst.* **12**, 126–129.
Frisch, M. J. *et al.* (2003). *GAUSSIAN*03, Revision B.04. Gaussian, Inc., Pittsburgh PA.
Grineva, O. V. & Zorkii, P. M. (1998). *Zh. Fiz. Khim.* **72**, 714–720 (in Russian).
Grineva, O. V. & Zorkii, P. M. (2001). *J. Struct. Chem.* **42**, 16–23.
Holler, A. (1947). *J. Org. Chem.* **13**, 10–14.
Housty, J. & Clastre, J. (1957). *Acta Cryst.* **10**, 695–698.
Ibberson, R. M. & Wilson, C. C. (2002). *J. Phys. Condens. Matter*, **14**, 7287–7295.
Katrusiak, A. (1999). *J. Appl. Cryst.* **32**, 1021–1023.
Katrusiak, A. (2003). *REDSHABS.* Adam Mickiewicz University, Poznań.
Katrusiak, A. (2004). *Z. Kristallogr.* **219**, 461–467.
Lide, D. R. (1994). Editor-in-Chief. *CRC Handbook of Chemistry and Physics*, 75th Ed. Boca Raton: CRC Press Inc.
McKinnon, J. J., Spackman, M. A. & Mitchell, A. S. (2004). *Acta Cryst.* B**60**, 627–668.
Merrill, L. & Bassett, W. A. (1974). *Rev. Sci. Instrum.* **45**, 290–294.
Murray, J. S., Paulsen, K. & Politzer, P. (1994). *Proc. Indian Acad. Sci. (Chem. Sci.)* **106**, 267–275.
Nyburg, S. C. & Faerman, C. H. (1985). *Acta Cryst.* B**41**, 274–279.
Oxford Diffraction (2004). *CrysAlisCCD* and *CrysAlisRED*, Versions 1.171.24 beta. Oxford Diffraction, Poland.
Piermarini, G. J., Block, S., Barnett, J. D. & Forman, R. A. (1975). *J. Appl. Phys.* **46**, 2774–2780.
Politzer, P., Murray, J. S. & Concha, M. C. (2002). *Int. J. Quant. Chem.* **88**, 19–27.
Powell, B. M., Heal, K. M. & Torrie, B. H. (1984). *Mol. Phys.* **53**, 929–939.
Price, S. L., Stone, A. J., Lucas, J., Rowland, R. S. & Thornley, A. E. (1994). *J. Am. Chem. Soc.* **116**, 4910–4918.
Sankaran, H., Sharma, S. M., Sikka, S. K. & Chidambaram, R. (1986). *Pramana J. Phys.* **27**, 835–839.
Sheldrick, G. M. (1990). *SHELXTL.* Siemens Analytical X-ray Instrument Inc., Madison, Wisconsin, USA.
Sheldrick, G. M. (1997). *SHELX*97. University of Göttingen, Germany.
Slovokhotov, Y. L., Neretin, I. S. & Howard, J. A. K. (2004). *New. J. Chem.* **28**, 967–979.
Spackman, M. A. & McKinnon, J. J. (2002). *CrystEngComm*, **4**, 378–392.
Stevens, E. D. (1979). *Mol. Phys.* **37**, 27–45.
Thiéry, M.-M. & Rérat, C. (2003). *J. Chem. Phys.* **118**, 11100–11110.
Tomoda, S., Takamatsu, K. & Iwaoka, M. (1998). *Chem. Lett.* **27**, 581–582.
Vos, W. L., Finger, L. W., Hemley, R. J. & Mao, H. (1993). *Phys. Rev. Lett.* **71**, 3150–3153.
Wheeler, G. L. & Colson, S. D. (1975). *Acta Cryst.* B**31**, 911–913.
Wheeler, G. L. & Colson, S. D. (1976). *J. Phys. Chem.* **65**, 1227–1235.
Wolff, S. K., Grimwood, D. J., McKinnon, J. J., Jayatilaka, D. & Spackman, N. A. (2005). *CrystalExplorer*, Version 1.5.0. University of Western Australia.